Probing the Nucleotide Binding Domain of the Osmoregulator EnvZ Using Fluorescent Nucleotide Derivatives†

Leigh Plesniak,‡ Yuki Horiuchi,§ Daniel Sem,|| David Meinenger,|| Linda Stiles,|| Jennifer Shaffer,⊥ Patricia A. Jennings,§ and Joseph A. Adams*,⊥

Department of Pharmacology and Department of Chemistry & Biochemistry, University of California, San Diego, La Jolla, California 92093-0506, Department of Chemistry, University of San Diego, San Diego, California, and Triad Therapeutics, Inc., San Diego, California 92121

Received May 2, 2002

ABSTRACT: EnvZ is a histidine protein kinase important for osmoregulation in bacteria. While structural data are available for this enzyme, the nucleotide binding pocket is not well characterized. The ATP binding domain (EnvZB) was expressed, and its ability to bind nucleotide derivatives was assessed using equilbrium and stopped-flow fluorescence spectroscopy. The fluorescence emission of the trinitrophenyl derivatives, TNP-ATP and TNP-ADP, increase upon binding to EnvZB. The fluorescence enhancements were quantitatively abolished in the presence of excess ADP, indicating that the fluorescent probes occupy the nucleotide binding pocket. Both TNP-ATP and TNP-ADP bind to EnvZB with high affinity (K_d = 2−3 μM). The TNP moiety attached to the ribose ring does not impede access of the fluorescent nucleotide into the binding pocket. The association rate constant for TNP-ADP is 7 μM^{-1} s^{-1}, a value consistent with those for natural nucleotides and the eucaryotic protein kinases. Using competition experiments, it was found that ATP and ADP bind 30- and 150-fold more poorly, respectively, than the corresponding TNP-derivatized forms. Surprisingly, the physiological metal Mg^{2+} is not required for ADP binding and only enhances ATP affinity by 3-fold. Although portions of the nucleotide pocket are disordered, the recombinant enzyme is highly stable, unfolding only at temperatures in excess of 70 °C. The unusually high affinity of the TNP derivatives compared to the natural nucleotides suggests that hydrophobic substitutions on the ribose ring enforce an altered binding mode that may be exploited for drug design strategies.

The ability to detect and transduce external signals into intracellular information is essential for cell growth and survival. This process, known as signal transduction, relies partly on the action of protein kinases to phosphorylate specific targets within signaling cascades. While eucaryotic cells use primarily serine/threonine- and tyrosine-specific protein kinases for these purposes, prokaryotic cells often rely on histidine protein kinases (HPKs)[1] to respond to environmental conditions or stresses (*1*−*3*). Each HPK operates within a two-component signaling system where the kinase transfers the γ phosphate of ATP to a specific histidine within the HPK and this phosphate moiety is then shuttled to an aspartate residue on the signaling partner or response regulator (RR) (*3*, *4*). The RR's function (enzymatic, DNA binding, etc.) is altered as a result of phosphorylation allowing the organism to adjust to environmental changes. Thus, the HPKs may serve as a first line of defense for a pathogen when challenged with antimicrobial agents or other harmful agents. The HPKs are abundant (with 30 identified HPKs in *Eschericia coli*, *5*) and structurally distinct from the serine, threonine, and tyrosine kinases of eucaryotic systems. The structural diversity from eucaryotic protein kinases [ePKs], predominance in prokaryotic organisms, and links to the emerging resistance to existing antibiotic treatment in *Streptococcus pneumoniae* (*6*, *7*) make them potential targets for new antibiotic therapeutics.

Structural and functional studies have revealed that HPKs are modular and possess specific signature sequence motifs. The homologous sequences are termed H, N, G1, F, and G2 boxes (*2*, *8*) (Figure 1A). The H box contains the substrate histidine, while N, G1, F, and G2 boxes are conserved sequences located within the ATP binding domain. The HPKs are grouped into two subclasses according to the organization of these sequences into functional domains (*9*). Class I histidine kinases have the conserved H box located in a domain immediately amino terminal to the N, G1, F, and G2 boxes. In class II histidine kinases, the H box is

† The work in the manuscript was supported by a BioSTAR award (B99-52) and an NSF grant (111068).

* Corresponding author. Tel.: (858) 822-3360. Fax: (858) 822-3361. E-mail: joeadams@ucsd.edu.

‡ Department of Chemistry, University of San Diego.

§ Department of Chemistry & Biochemistry, University of California, San Diego.

|| Triad Therapeutics, Inc.

⊥ Department of Chemistry & Biochemistry, University of California, San Diego.

[1] Abbreviations: ADP, adenosine 5′-disphosphate; AMP-PNP, β,γ-imidoadensoine-5′-triphosphate; ATP, adenosine 5′-triphosphate; CD, circular dichroism; EnvZB, ATP binding domain of EnvZ; ePK, eucaryotic protein kinase; HPK, histidine protein kinase; IPTG (isopropyl β-D-thiogalactoside); Ni−NTA, nickel−nitriloacetic acid; RR, response regulator; TNP-ADP, 2′(3′)-*O*-(trinitrophenyl)adenosine 5′-disphosphate, disodium salt; TNP-ATP, 2′(3′)-*O*-(trinitrophenyl)-adenosine 5′-triphosphate, trisodium salt.

10.1021/bi020331j CCC: $22.00
Published on Web 10/29/2002

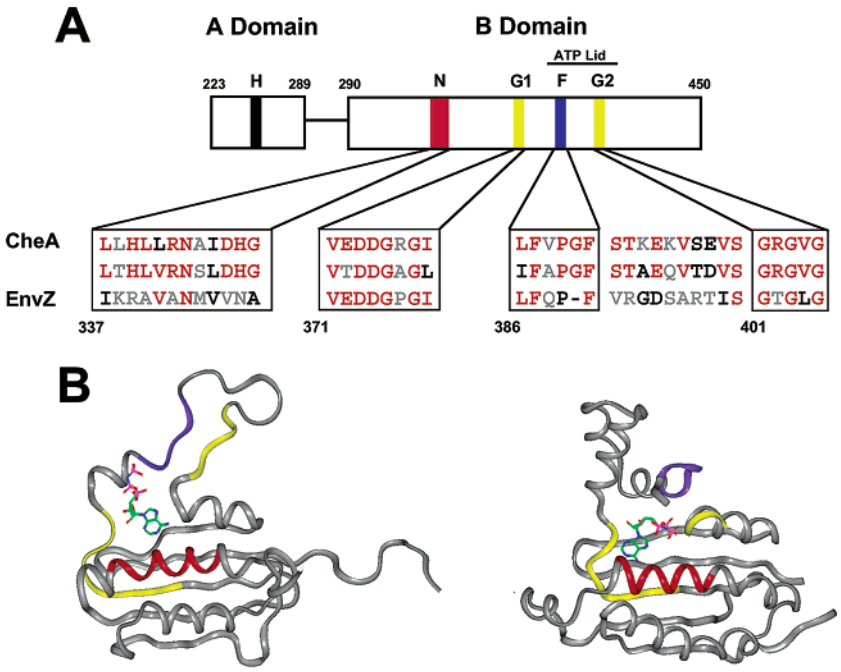

FIGURE 1: Primary and tertiary structures of EnvZ and CheA. **(**A) An alignment of the N box (red), G1 box (yellow), F box (blue), and G2 box (yellow) sequence motifs of CheA isolated from *Thermatoga maritima* (top*)* and *E. coli* (middle) and EnvZ from *E. coli* (bottom). The H box containing the acceptor histidine is located in the A domain of EnvZ. The numbers reflect positions in the sequence of EnvZ. (B) Ribbon diagrams of the ATP binding domains of EnvZB (left) and CheA (right) in complex with AMPPNP. The ribbons are colored according to the sequence motifs in panel A.

separated from the remaining sequence motifs by a domain and is located in an amino terminal region. The osmoregulator EnvZ and the chemotaxis protein, CheA, serve as paradigms for the class I and class II families of HPKs, respectively. Crystal structures of the kinase and regulatory domains of CheA isolated from *Thermatoga maritima*, have been solved in the free form (*9*) and the ATP-binding domain solved in the presence of nucleotide analogues (*10*). An NMR structure of the AMPPNP-bound kinase domain of EnvZ [EnvZB] has also been solved (*11*) (Figure 1B). These structures provide insights into protein:ligand interactions that occur upon binding of nucleotide analogues and reveal that the conserved G1, N, G2, and F boxes surround the nucleotide-binding pocket.

With the emergence of bacterial strains resistant to the standard regimen of antimicrobial agents, there are pressing demands for new approaches toward controlling the growth of virulent bacteria. Since HPKs are predominantly expressed in prokaryotes rather than eucaryotes, inhibitors of this enzyme family offer the exciting possibility of attaining selective toxicity in the parasitic organism (*12*). The ePKs can be inhibited selectively by drugs that are largely nucleotide-directed (*13*). Indeed, an approved drug for the treatment of chronic myleogenous leukemia (CML) is directed at inhibiting the protein kinase BCR-Abl through interactions in the nucleotide pocket. It is likely that this selectivity is achieved by utilizing the common hydrophobic pocket for the adenine ring of ATP in addition to unique regions outside this pocket (*13*). Such approaches shown to be successful with the ePKs may be applicable to the HPKs. Thus, it is important to understand the nucleotide binding pockets in this enzyme family. In this manuscript, we have characterized the nucleotide binding domain of the osmoregulator EnvZ using the fluorescent analogues TNP-ATP and TNP-ADP. We have shown that the binding of both of these derivatives can be monitored using equilibrium and stopped-flow fluorescence spectroscopy. While these ligands effectively compete for the natural nucleotides, as expected, they bind in altered modes utilizing unique surfaces in the active site. These differences are manifested in unusually high affinities of the derivatives compared to the natural nucleotides and in the abolishment of a metal ion dependence linked to the γ phosphate of ATP.

MATERIALS AND METHODS

Materials. 2′(3′)-*O*-(trinitrophenyl)adenosine 5′-disphosphate (TNP-ADP) and 2′(3′)-*O*-(trinitrophenyl)adenosine 5′-triphosphate were purchased from Molecular Probes, Inc. (Eugene, OR). ADP and ATP were purchased from Sigma-Aldrich (St. Louis, MO).

Protein Expression and Purification. The kanamycin resistance marker of plasmid pET28a (Novagen) was exchanged for the ampicillin resistance marker of pET21a using the unique A1wN1 and Xho1 restriction sites of each plasmid, generating plasmid ApET28a. Synthetic oligonucleotides corresponding to both strands of a DNA cassette encoding a hexahistidine tag upstream from a Prescission Protease (Amersham Biosciences) recognition sequence were designed with the termini of each oligonucleotide corresponding to a 5′ Nco1 and 3′ Nde1 restriction product. These olionucleotides were annealed, phosphorylated, and ligated into ApET28a via the unique 5′ Nco1 and 3′ Nde1 restriction sites, generating the custom plasmid APpET28a. DNA encoding the B domain (residues 289−450) of EnvZ was cloned from the genomic DNA of a K12-derived strain of *E. coli*. The PCR product was subcloned into the APpET28a expression vector through the BamH1 and EcoR1 restriction sites, and the correct DNA sequence was verified.

The plasmid containing the B domain was transformed into *E. coli* BL21(DE3), grown at 37 °C with 50 μg/mL ampicillin, and induced for 4−5 h with 1 mM IPTG. Cell pellets, resuspended in 50 mM phosphate buffer (pH 8.0), 300 mM NaCl, 10 mM imidazole, were treated with 1 mg/mL lysozyme for 30 min on ice and then sonicated (Sonic Dismembrator 550, Fisher) with 30 s pulses separated by 30 s breaks for a total of 10 minutes. The lysate was cleared by centrifugation at 15 000 rpm for 30 min. The catalytic domain (EnvZB) was eluted from a Ni−NTA resin (Qiagen Inc.) using 50 mM phosphate buffer (pH 8.0), 300 mM NaCl, 250 mM imidazole. The histidine tag was removed using PreScission Protease (100 units) and the cleaved EnvZB was purified using a Sephacryl S-200 equilibrated with 20 mM Tris-HCl, pH 7.8, 250 mM NaCl, 5% glycerol, and 10 mM β-mercaptoethanol.

Circular Dichroism Spectroscopy. The secondary structure content and thermal stability of the EnvZB were analyzed using circular dichroism (CD) spectroscopy collected on an AVIV CD Spectrometer, Model 202 (Aviv Instruments, Inc. Lakewood, New Jersey) equipped with automated temperature control. Using 11 μM EnvZB in a rectangular cuvette with 0.1 cm path length, spectra were acquired from 190 to 260 nm. Thermal melts for EnvZB were carried out from 20 to 90 °C, stepping 2 °C with a 4 min equilibration time. Loss of secondary structure was monitored via changes in θ at 222 nm.

Fluorescence Spectroscopy. Fluorescence experiments were carried out on the Fluoromax-2 (Jobin Yvon-SPEX, Instruments S.A., Inc. Edison, NJ) equipped with a circulating water bath. Binding of trinitrophenyl derivatives of ATP and ADP was detected via a fluorescence enhancement in the presence of EnvZB at an excitation wavelength of 410 nm (excitation and emission slits were set to 2 and 4 nm, respectively). An initial 2 mL sample was prepared with 5 μM TNP-ADP in 50 mM Tris-HCl, pH 7.5, 10 mM β-mercaptoethanol [BME], and 10 mM $MgCl_2$, and an emission scan was acquired. EnvZB was then added directly to the cuvette to a final concentration of 1.1 μM, and the fluorescence spectrum was re-acquired. Finally, 5 mM ADP was added to monitor fluorophore displacement, with all spectral intensities corrected for dilution. Control experiments were carried out in the absence of EnvZB to ensure that ADP does not alter the fluorescence emission of TNP-ADP.

Titrations with TNP-ADP and TNP-ATP. Titrations of TNP-ADP and TNP-ATP were carried out, unless otherwise stated, in 10 mM $MgCl_2$, 50 mM Tris-HCl, pH 7.5, 10 mM BME with 1.1 μM EnvZB. Microliter quantities of TNP-ADP or TNP-ATP were titrated into 2 mL samples from stock solutions of fluorescent nucleotide. TNP concentrations were measured spectrophotometrically ($\epsilon_{408} = 26\,000\ cm^{-1}\ M^{-1}$). The samples were mixed for 1 min before data acquisition. Slits were set to 3 nm for excitation and 5 nm for emission. Changes in fluorescence intensity were monitored at 543 nm in 10 s intervals over 1 min, and average values were taken. A blank sample titration lacking EnvZB was carried out for each titration of TNP-ADP or TNP-ATP in the presence of protein.

ADP and ATP Displacement Experiments. Displacement experiments were carried out with samples containing 5 μM TNP-ADP, 10 mM $MgCl_2$, 50 mM Tris-HCl pH 7.5, 10 mM BME, and 1.1 μM EnvZB. Fluorescence intensity decrease was monitored as microliter quantities of concentrated ATP or ADP were added to the sample. For measurement of dissociation constants for ADP and ATP, TNP-ADP titrations were carried out, as described in the previous section, in the presence of 100, 200, or 400 μM ADP or ATP. In the ADP displacement experiments, excitation slits were set to 2 nm.

Analysis of Titration Data. The observed changes in fluorescence at any given concentration of TNP derivative (ΔF) were normalized to the total change in fluorescence at infinite concentration (ΔF_{max}) to obtain the ratio $\Delta F/\Delta F_{max}$. Data were fit to the quadratic equation below:

$$\frac{\Delta F}{\Delta F_{max}} = \frac{(K_d + L_t + E_t) - \sqrt{(K_d + L_t + E_t)^2 - 4L_tE_t}}{2E_t} \quad (1)$$

where L_t and E_t are the total concentrations of ligand and protein and K_d is the dissociation constant (*14*). For titration experiments in the presence of fixed amounts of competing nucleotides (ATP and ADP), the plots yield apparent K_d's [$^{app}K_d^{TNP}$]. The true K_d values for the competing ligands were then calculated using eq 2:

$$^{app}K_d^{TNP} = K_d^{TNP}\left(1 + \frac{[L]}{K_d^L}\right) \quad (2)$$

where [L] is the concentration of the competing nucleotides (ATP or ADP) and K_d^{TNP} and K_d^L are the dissociation constants for the TNP derivative and the natural nucleotide, respectively (*15*). Equation 2 was solved assuming that the total and free ligand concentrations are equivalent.

Stopped-Flow Fluorescence Spectroscopy. All transient-state kinetic measurements were obtained using an Applied Photophysics stopped-flow spectrometer. Samples were mixed in a 1:1 ratio with 50 μM TNP-ADP and 10 mM $MgCl_2$ in one syrine and 2 μM EnvZB and 10 mM $MgCl_2$ in the second syringe. The fluorescence emission was measured using a 420 nm cuton filter. The instrument collected a total of 400 data points for 50 ms in each experiment. For data analysis, the average of 5−10 individual traces was used. The fluorescence data were recorded as millivolts, and the time data were corrected for the instrument deadtime by adding 1.5 ms to all the time points. Rate constants and amplitudes were obtained by fitting of the data to equations describing a single-exponential growth using the computer program KaliedaGraph (Synergy Software).

RESULTS

Circular Dichroism Studies. Key binding determinants within the kinase domain lie in a highly disordered loop in the NMR structure of the AMPPNP:EnvZB complex (*11*, *16*) and may suggest that the domain is partially unfolded when excised from the dimerization domain (Figure 1B). To assess whether this domain is cooperatively folded, changes in secondary structure as a function of temperature were evaluated by far-UV CD spectroscopy. EnvZB exhibits the characteristic double minima spectra (222 and 209 nm) expected for an α/β protein, (Figure 2A). The stability of the kinase domain was assessed by monitoring the CD signal at 222 nm as a function of temperature (Figure 2B). The domain is highly stable to changes in solution temperature, with no significant changes in CD signal apparent up to ~70

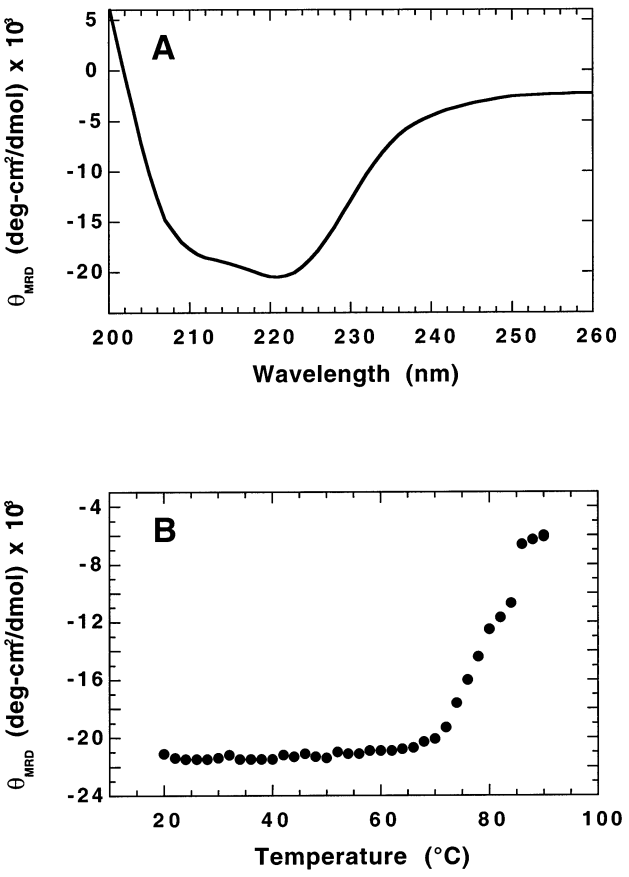

FIGURE 2: Structural Stability of EnvZB. (A) CD spectrum of EnvZB. Protein (11 μM) was scanned between 200 and 260 nm. (B) Temperature melt. The CD spectra were recorded at 2 degree intervals from 20 to 90 °C.

°C. Above 70 °C, a cooperative transition in the CD signal is observed and is indicative of the unfolding of the domain with a thermal midpoint of approximately 80 °C.

Nucleotide Analogue Binding Affinities. Fluorescent analogues of ATP and ADP were used as probes to characterize nucleotide binding to EnvZB. TNP-ADP and TNP-ATP have ether-linked trinitrophenyl groups attached to the 2′ and 3′ ribose oxygens and are weakly fluorescent in aqueous solution. These compounds exhibit an enhancement in fluorescence intensity when sequestered from aqueous solvent upon binding to buried (or partially buried) sites within target proteins (*10*, *15*). Plots of the fluorescence intensity as a function of wavelength for a solution of TNP-ADP (5 μM) in the presence and absence of added enzyme are given in Figure 3A. Addition of EnvZB to the TNP-ADP solution results in a nearly 3-fold increase in fluorescence intensity, indicating that an EnvZB:TNP-ADP complex was formed. Subsequent addition of excess ADP produced a fluorescence spectrum that was indistinguishable from the TNP-ADP spectrum, indicating that TNP-ADP and ADP compete for the same binding site (Figure 3A). Nucleotide-analogue binding affinities were assessed with equilibrium fluorescence methods. Plots of the relative fluorescence intensities ($\Delta F/\Delta F_{max}$) as a function of nucleotide concentration reveal smooth binding isotherms for both TNP-ATP and TNP-ADP in the presence of 10 mM $MgCl_2$ (Figure 3B). The data are fit to eq 1 and the K_d values are listed in Table 1. Similar fluorescence titration experiments were also performed in the absence of Mg^{2+} (data not shown). By

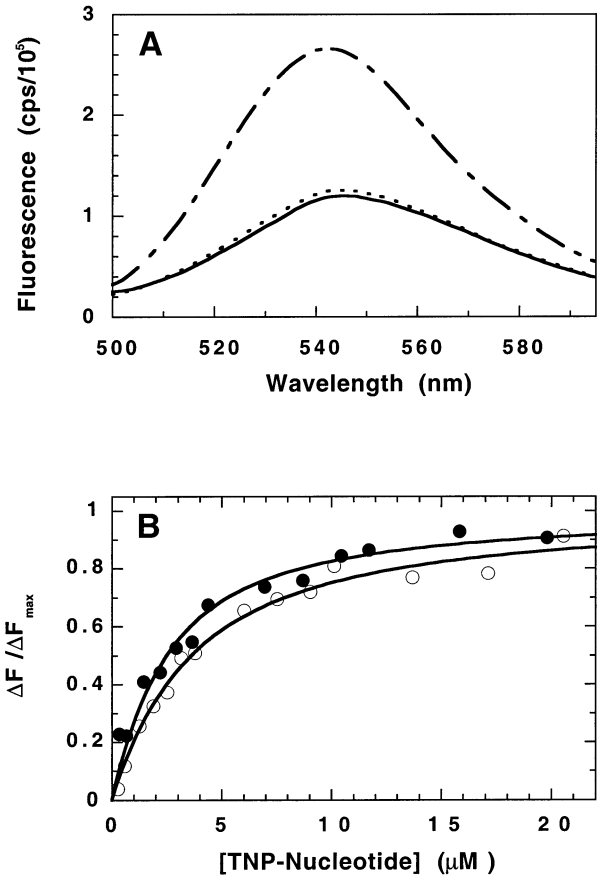

FIGURE 3: Equilibrium binding of TNP derivatives to EnvZB using fluorescence spectroscopy. (A) Fluorescence spectra of 5 μM TNP-ADP (—), 5 μM TNP-ADP in the presence of 1.1 μM EnvZ (— - —), and 5 μM TNP-ADP in the presence of 1.1 μM EnvZ and 5 mM ADP (---). (B) Titration of EnvZB with TNP-ATP (○) and TNP-ADP (●). Changes in relative fluorescence emission at 543 nm are monitored as a function of total ligand concentration using 1.1 μM EnvZB. The data were fitted to eq 1 and the K_d values are listed in Table 1.

Table 1: Dissociation Constants for the TNP Derivatives and Natural Nucleotides to EnvZB and CheA

	K_d (μM)	
ligand	EnvZB	CheA[a]
TNP-ATP	1.9 ± 0.3	0.5
TNP-ADP	3.0 ± 0.4	0.4
ATP	60 ± 10	260
ADP	300 ± 50	90
ATP/ADP[b]	5	0.4

[a] The K_d's correspond to K_{d1}'s reported in ref *15*. [b] ATP/ADP is the ratio of K_d's for ADP and ATP. Values greater than 1 imply that ATP binds better than ADP. Values less than 1 imply that ADP binds better than ATP.

monitoring relative increases in fluorescence, K_d values of 1.0 ± 0.2 and 1.8 ± 0.2 μM were determined for TNP-ATP and TNP-ADP, respectively. These values are similar to the K_d's for the TNP derivatives in the presence of Mg^{2+} (Table 1).

Kinetics of TNP-ADP Binding. The binding of TNP-ADP to EnvZB was monitored using stopped-flow techniques to determine the association kinetics of this derivative. Using 25 μM TNP-ADP, a rapid rise in fluorescence is observed (Figure 4) within the first 15 ms of the transient. The transient was fitted to an exponential function with an observed rate

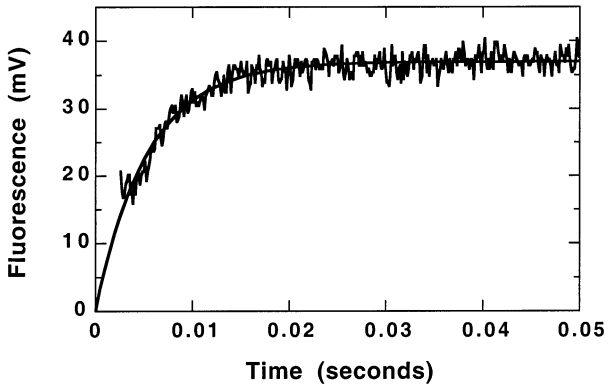

FIGURE 4: Stopped-flow kinetic binding of TNP-ADP to EnvZ. EnvZ (1 μM) is mixed with TNP-ADP (25 μM) in the presence of 10 mM $MgCl_2$. The data were fitted to a single-exponential function with an observed rate constant of 200 s^{-1}.

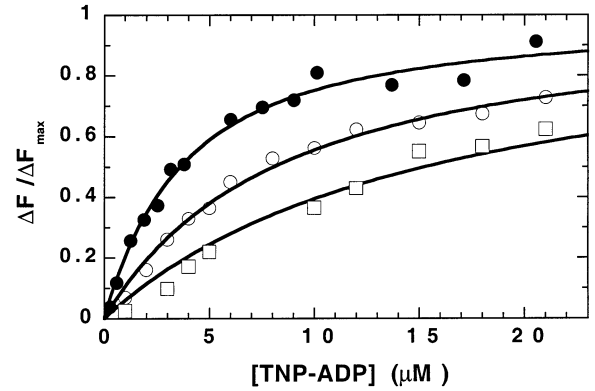

FIGURE 5: Binding of TNP-ADP in the presence of ATP. Relative fluorescence changes are monitored upon the addition of varying TNP-ADP concentrations to EnvZ (1.1 μM) with 0 μM (●), 100 μM (○), and 200 μM (□) ATP.

constant of 200 s^{-1}. Poor fluorescence output prevented measurement of transients below 25 μM TNP-ADP. Also, above this concentration significant losses in amplitude and high backgrounds owing to the fluorescence of the free ligand made it impossible to measure accurately a ligand dependence on the observed rate. Nonetheless, the apparent rate in Figure 4 permits an estimate of the association rate constant (k_{on}), assuming that TNP-ADP binds in a single bimolecular step. Is so, the observed rate of binding (k_{obs}) is related to the total ligand concentration when [L] > [E] by the following relationship: $k_{obs} = k_{on}[L] + k_{off}$ (*17*). Using the thermodynamic definition of K_d ($K_d = k_{off}/k_{on}$), k_{on} can be estimated from k_{obs} and the total ligand concentration by the following relationship: $k_{on} = k_{obs}/([L] + K_d)$. Using this rationale, an association rate constant of 7 μM^{-1} s^{-1} is attained for TNP-ADP. While this treatment of the data assumes a simple one-step binding mechanism which has not been confirmed, the observed rate fit in Figure 4 sets an upper limit of 8 μM^{-1} s^{-1} (200s^{-1}/25 μM) for k_{on}, a value close to this estimation (*17*).

Natural Nucleotide Binding Affinities. Since the data in Figure 3 indicate that the natural nucleotide, ADP, can abrogate the fluorescence increase observed with TNP-ADP, we performed titration experiments in the presence of the natural nucleotides to attain K_d values. In these experiments, EnvZB is titrated with TNP-ADP in the absence and presence of varying, fixed concentrations of the natural nucleotide. As shown in Figure 5, the presence of 100 and 200 μM ATP has profound effects on the binding of TNP-ADP, making it progressively more difficult to saturate the enzyme in the presence of higher concentrations of the competitor. Using eq 1, apparent K_d values of 7.5 ± 0.2 and 14.7 ± 1.0 μM are attained at 100 and 200 μM ATP. Using eq 2 and the K_d for TNP-ADP in the absence of ATP, an average K_d for ATP of 60 μM is obtained. Similar experiments were performed with ADP as the competitor (data not shown). The resulting K_d values for ATP and ADP are displayed in Table 1. These studies indicate that TNP-ATP binds about 30-fold better than ATP whereas TNP-ADP binds about 100-fold better than ADP.

Effects of Magnesium on Natural Nucleotide Binding. While the binding of TNP-ADP and TNP-ATP is not affected significantly by the presence of Mg^{2+}, the higher affinities of the fluorescent derivatives (Table 1) suggest that they may utilize an altered binding mode. To monitor the role of Mg^{2+}

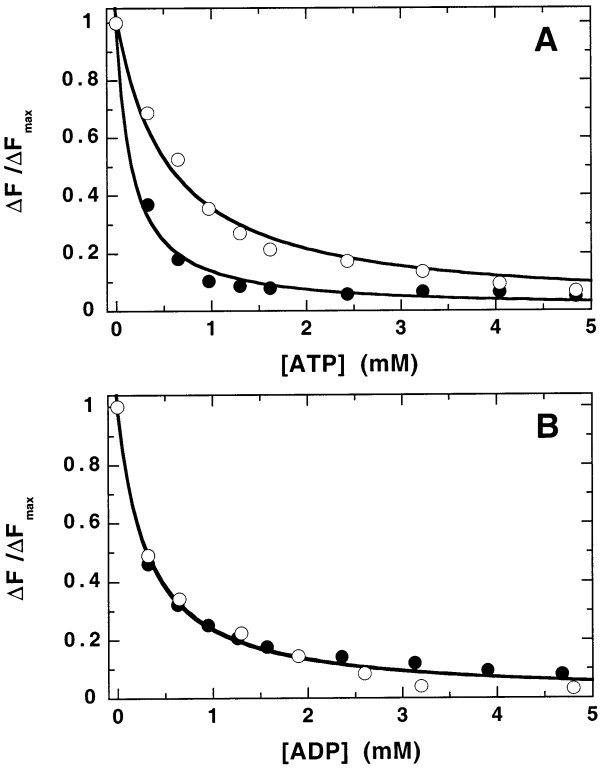

FIGURE 6: Displacement of TNP-ADP from EnvZB using ATP (A) and ADP (B). The relative fluorescence of EnvZ (1.1 μM) preequilibrated with TNP-ADP (5 μM) is monitored as a function of varying concentrations of ATP and ADP in the absence (○) and presence of 10 mM $MgCl_2$ (●).

in controlling the affinity of the natural nucleotides, displacement experiments were performed. In these experiments, EnvZ (1 μM) is preequilibrated with TNP-ADP (5 μM) prior to addition of increasing concentrations of ATP and ADP in the presence and absence of Mg^{2+}. The resulting displacement curves are displayed in Figure 6. The apparent association constants for ATP are 1.9 and 6.2 mM^{-1} in the absence and presence of Mg^{2+}. In comparison, the apparent association constant for ADP is 3.2 mM^{-1} in both the presence and absence of Mg^{2+}. While these association constants are not corrected for the concentration of TNP-ADP, relative changes in these values are comparable since the fluorophore concentration is kept constant in all displacement experiments. These data imply that the affinity of ATP

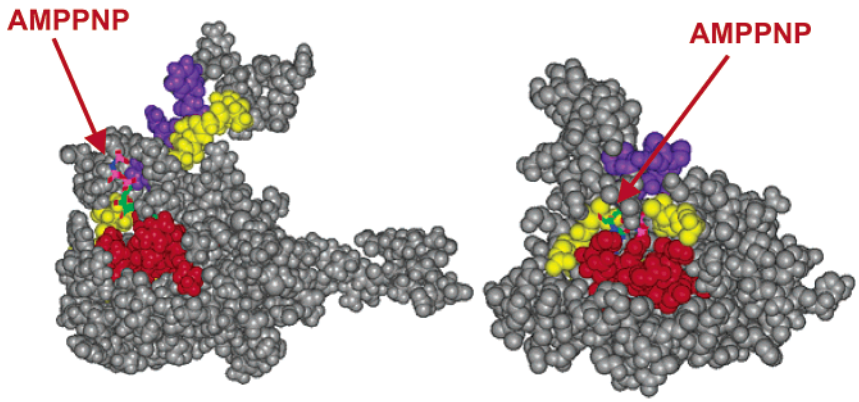

FIGURE 7: Spacefilling models of EnvZB (left) and CheA (right) in complex with AMPPNP colored according to sequence motifs, N box (red), G1 and G2 boxes (yellow), and F box (blue) (see Figure 1A).

is increased by about 3-fold in the presence of 10 mM Mg^{2+} whereas the affinity of ADP is unaffected by the divalent metal ion.

DISCUSSION

The catalytic domains of the procaryotic HPKs are easily differentiated from those of the ePK family. All members of the ePK family share a conserved kinase core capable of binding both ATP and substrate protein (*18*). This core is composed of an ATP binding subdomain rich in β strands and a substrate binding subdomain rich in α helices (*18*). In comparison, the ATP binding domains of the HPKs are composed of an α/β sandwich with a distinctive unstructured loop region (Figure 1). In the HPKs, the adenine portion of the nucleotide binds in a hydrophobic region near the β strands. The γ phosphate of ATP is highly solvent exposed and poised for delivery to the histidine of the acceptor domain. Despite these similarities within the catalytic domains of the HPKs, several conserved sequences in the class I and II families lie in different regions of the folded structures. For example, the two conserved regions in the ATP lid (F and G2; Figure 1) lie in different orientations in the folded proteins. Such differences may be important for the development of selective agents against the class I and II enzymes. In this manuscript we have defined several unique features of the EnvZ ATP binding domain using fluorescence spectroscopy and nucleotide derivatives.

Structural Stability of the ATP Binding Domain. The structure of the ATP binding domain of EnvZ is unusual due to the presence of a large unstructured region (Figure 1). Given this unusual conformation, we wished to determine the stability of our recombinantly expressed EnvZB using temperature melts. As shown in Figure 2, the ATP binding domain is highly stable and resistant to denaturation up to 70 °C. Above this threshold, however, the protein cooperatively unfolds, as evidenced by large, distinct changes in the CD spectra. The overall stability of EnvZB may result from the high stability of the α/β sandwich motif. In comparison, the catalytic domain of cAMP-dependent protein kinase, a ePK, loses structural content at much lower temperatures (*19*) despite the absence of any large disordered regions in the X-ray structure (*20*).

TNP as a Fluorescent Probe for EnvZ. The substitution of TNP at the 2′(3′) hydroxyls of ATP and ADP generates fluorescent nucleotides that alter their fluorescence emission spectra upon binding to EnvZB. The resulting derivatives, TNP-ATP and TNP-ADP, bind reversibly and with high affinity to the nucleotide pocket (Figure 3 and Table 1). The observed K_d's are close in value to those measured for the CheA dimer using the identical nucleotide derivatives (*15*). While kinases typically utilize divalent metal ions for nucleotide binding, both TNP-ATP and TNP-ADP bind with equivalent affinities in either the presence or absence of $MgCl_2$ (Table 1). This result stands in contrast to that observed with the ePKs which do not bind ATP or ADP well in the absence of divalent metal ions (*21*). While there is likely a role for metal ions in assisting the binding of natural nucleotides to EnvZ, the TNP derivatives likely utilize different interactions in the nucleotide pocket, which dominate over electrostatic contacts near the triphosphate region.

Energy Contribution From the Fluorophore. Fluorescently labeled nucleotide derivatives have been used previously to probe nucleotide binding in several ePKs (*22*, *23*). In general, attachment of a methylanthraniloyl ring to the 2′(3′) hydroxyl of ATP and ADP (mant derivatives) either has no affect or lowers the affinity of the nucleotide relative to the natural ligand. In comparison, attachment of the TNP moiety to ATP and ADP increases the affinity of the nucleotides by 30- to 100-fold relative to the underivatized ligands (Table 1). These findings support the notion that the TNP ring enhances affinity by recognizing additional residues in or near the nucleotide pocket. These unique interactions clearly take priority over any effects of the γ phosphate on nucleotide binding. Indeed, when the TNP moieties are removed, there is a clear 5-fold difference in the binding affinities of ATP and ADP (Table 1). Finally, the higher affinity of ATP relative to ADP suggests that the γ phosphate makes a favorable contact with, at least, one residue in the active site.

Is There a Role for Metal Ions in Supporting Nucleotide Binding? In the ePKs, Mg^{2+} plays an essential role in chelating the γ phosphate of ATP and supporting phosphoryl transfer to protein substrates. To determine whether the presence of Mg^{2+} supports the binding of either ATP or ADP, TNP-ADP displacement experiments were performed in the presence and absence of $MgCl_2$ (Figure 6). While Mg^{2+} has no effect on the binding of ADP, the divalent metal activator enhances the affinity of ATP by approximately 3-fold. We conclude from these studies that the γ phosphate of ATP interacts with Mg^{2+} and an active-site residue facilitating the association of the phosphoryl donor. While these results delineate a clear role for metal ion in the active site, the overall enhancement offered by the metal is relatively small

compared to those effects observed with the ePKs (*21*). The high solvent accessibility of the γ phosphate in the EnvZB structure (Figure 1) may underlie the abbreviated influence of Mg^{2+}.

Comparison of EnvZ and CheA. Through displacement experiments, we showed that EnvZB binds ATP with higher affinity than ADP (Table 1). This contrasts sharply with CheA, where ADP binding is preferred to ATP binding. The K_d's for ADP to the two binding sites in Che A are 90 and 330 μM (*15*). In comparison, the K_d's for ATP to these two sites are 260 μM and 1.1 mM (*15*). The two binding sites within a CheA dimer were shown to be separate and noninteracting with equal affinity for nucleotide. The second K_d reflects statistical occupancy of the second site on a given dimer. Thus, only the first K_d listed in Table 1 corresponds to the nucleotide affinity in the CheA monomer. While it may be possible that dimerization of EnvZ influences nucleotide specificity, it is also possible that the structural differences between EnvZ and CheA near the triphosphate region accounts for these differences.

A comparison of the space-filling models of the catalytic domains for the two prototypic HPKs (CheA and EnvZ) reveal that the nucleotides bind very differently (Figures 1B and 7). The adenine ring of ATP is more deeply embedded in the pocket closer to the β sheet of CheA. Also, the triphosphate moiety of ATP is positioned differently in the two enzymes. The authors caution that relatively few distance constraints orient the nucleotide in the ATP-binding pocket. Nonetheless, these structural differences may explain some of the unique binding properties of EnvZB and provide grounds for developing inhibitors specific not only for the eucaryotic and prokaryotic protein kinases but also for the separate classes of HPKs.

The crystal structures of CheA in complex with TNP-ATP and AMPPNP have recently been solved and illustrate a different mode of binding for the trinitro-phenyl derivatives of ADP and ATP (*10*). In these structures, TNP-ATP and AMPNP have similar placement of the adenine base in the hydrophobic cleft. However, the ribose of TNP-ATP adopts an orientation that promotes interaction between the trinitrophenyl moiety and several hydrophobic side chains. This placement of the ribose projects the three phosphates into a more solvent-exposed position relative to the AMPPNP nucleotide, explaining the magnesium independence of binding to CheA. Of the five side chains interacting with the TNP moiety, one appears in a highly conserved position in the F box. The remaining four amino acids are in nonconserved regions flanking the loop. Whether a similar orientation for the TNP moieties in EnvZB occurs awaits a high-resolution structure. Nonetheless, differences in the primary sequence of EnvZ and in the loop structure may be utilized for the design of inhibitors with specificity for the HPK classes.

REFERENCES

1. Stock, A. M., Robinson, V. L., and Goudreau, P. N. (2000) *Annu. Rev. Biochem. 69*, 183-215.
2. Swanson, R. V., Alex, L. A., and Simon, M. I. (1994) *Trends Biochem. Sci. 19*, 485−490.
3. Egger, L. A., Park, H., and Inouye, M. (1997) *Genes Cells 2*, 167−84.
4. Alex, L. A., and Simon, M. I. (1994) *Trends Genet. 10*, 133 138.
5. Mizuno, T. (1999) *Tanpakushitsu Kakusan Koso 44*, 412−20.
6. Guenzi, E., Gasc, A.-M., Sicard, M. A., and Hakenbeck, R. (1994) *Mol. Microbiol. 12*, 505−515.
7. Novak, R., Henriques, B., Charpentier, E., Normark, S., and Tuomanen, E. (1999) *Nature 399*, 590−593.
8. Parkinson, J. S., and Kofoid, E. C. (1992) *Annu. Rev. Genet. 26*, 71−112.
9. Bilwes, A. M., Alex, L. A., Crane, B. R., and Simon, M. I. (1999) *Cell 96*, 131−41.
10. Bilwes, A. M., Quezada, C. M., Croal, L. R., Crane, B. R., and Simon, M. I. (2001) *Nat. Struct. Biol. 8*, 353−60.
11. Tanaka, T., Saha, S. K., Tomomori, C., Ishima, R., Liu, D., Tong, K. I., Park, H., Dutta, R., Qin, L., Swindells, M. B., Yamazaki, T., Ono, A. M., Kainosho, M., Inouye, M., and Ikura, M. (1998) *Nature 396*, 88−92.
12. Matsushita, M., and Janda, K. D. (2002) *Bioorg. Med. Chem. 10*, 855−67.
13. Cohen, P. (1999) *Curr. Opin. Chem. Biol. 3*, 459−65.
14. Taira, K., and Benkovic, S. J. (1988) *J. Med. Chem. 31*, 129−37.
15. Stewart, R. C., VanBruggen, R., Ellefson, D. D., and Wolfe, A. J. (1998) *Biochemistry 37*, 12269−79.
16. Tomomori, C., Tanaka, T., Dutta, R., Park, H., Saha, S. K., Zhu, Y., Ishima, R., Liu, D., Tong, K. I., Kurokawa, H., Qian, H., Inouye, M., and Ikura, M. (1999) *Nat. Struct. Biol. 6*, 729−34.
17. Johnson, K. A. (1992) in *The Enzymes* (Sigman, D. S., Ed.) pp 2−61, Academic Press, Inc., San Diego.
18. Taylor, S. S., Zheng, J., Radzio-Andzelm, E., Knighton, D. R., Ten Eyck, L. F., Sowadski, J. M., Herberg, F. W., and Yonemoto, W. M. (1993) *Philos. Trans. R. Soc. London, Ser. B: Biol. Sci. 340*, 315−24.
19. Herberg, F. W., Zimmermann, B., McGlone, M., and Taylor, S. S. (1997) *Protein Sci. 6*, 569−79.
20. Madhusudan, Trafny, E. A., Xuong, N. H., Adams, J. A., Ten Eyck, L. F., Taylor, S. S., and Sowadski, J. M. (1994) *Protein Sci. 3*, 176−87.
21. Adams, J. A. (2001) *Chem. Rev. 101*, 2271−2290.
22. Ni, Q., Shaffer, J., and Adams, J. A. (2000) *Protein Sci. 9*, 1818−27.
23. Jan, A. Y., Johnson, E. F., Diamonti, A. J., Carraway, I. K., and Anderson, K. S. (2000) *Biochemistry 39*, 9786−803.

BI020331J